Self-Assembly Behavior of pH- and Thermosensitive Amphiphilic Triblock Copolymers in Solution: Experimental Studies and Self-Consistent Field Theory Simulations

Chunhua Cai, Liangshun Zhang, Jiaping Lin,* and Liquan Wang

Key Laboratory for Ultrafine Materials of Ministry of Education, School of Materials Science and Engineering, East China University of Science and Technology, Shanghai 200237, China

Received: June 9, 2008; Revised Manuscript Received: August 1, 2008

We investigated, both experimentally and theoretically, the self-assembly behaviors of pH- and thermosensitive poly(L-glutamic acid)-*b*-poly(propylene oxide)-*b*-poly(L-glutamic acid) (PLGA-*b*-PPO-*b*-PLGA) triblock copolymers in aqueous solution by means of transmission electron microscopy (TEM), scanning electron microscopy (SEM), dynamic light scattering (DLS), circular dichroism (CD), and self-consistent field theory (SCFT) simulations. Vesicles were observed when the hydrophilic PLGA block length is shorter or the pH value of solution is lower. The vesicles were found to transform to spherical micelles when the PLGA block length increases or its conformation changes from helix to coil with increasing the pH value. In addition, increasing temperature gives rise to a decrease in the size of aggregates, which is related to the dehydration of the PPO segments at higher temperatures. The SCFT simulation results show that the vesicles transform to the spherical micelles with increasing the fraction or statistical length of A block in model ABA triblock copolymer, which corresponds to the increase in the PLGA length or its conformation change from helix to coil in experiments, respectively. The SCFT calculations also provide chain distribution information in the aggregates. On the basis of both experimental and SCFT results, the mechanism of the structure change of the PLGA-*b*-PPO-*b*-PLGA aggregates was proposed.

Introduction

Amphiphilic block or graft copolymers have been found to form self-assembled supramolecular structures in selective solvents. A variety of morphologies such as spheres, rods, vesicles, spindles, tubules, cylinders, toroids, and other complex structures have been observed.[1−9] These structures formed in aqueous media have attracted widespread interest for their potential applications in drug delivery systems, coatings, cosmetics, and nanoreactors.[10−13] An important issue toward making these self-assembled systems useful for specific applications is their capability to respond to external stimuli such as pH and temperature.[14−16] These sensitive self-assemblies, so-called "smart" micelles, show structure dependence on the external stimuli. Many studies have been done to explore the "smart" micelles, based on either single or mixed copolymer self-assembly systems.[17−25] For example, poly(acrylic acid)-*b*-poly(*N*,*N*-diethylacrylamide) (PAA-*b*-PDEAAm) was found to form pH- and thermoresponsive micelles in aqueous solution.[18] At lower temperatures and higher pH value conditions, the block copolymer is dissolved well in solution; when increasing the temperature or decreasing the pH value, micelles are formed with PDEAAm or PAA as core, respectively.

In the past few years, increasing attention has been paid to the polypeptide-based self-assemblies, because they have excellent biocompatibility and show significant advantages in controlling both the function and structures of the supramolecular self-assemblies. Polypeptides can serve as either hydrophilic[26−36] or hydrophobic[37−40] segments in amphiphilic copolymers. In some special cases, both hydrophilic and hydrophobic segments are polypeptides.[41−43]

It is well-known that polypeptides show various secondary structures, such as α-helix and random coil. The conformation adopted by the polypeptides depends on solvent, temperature, etc. For example, poly(L-glutamic acid) (PLGA) takes a coil conformation under basic conditions. As the pH value decreases, the coil conformation transforms to helix; meanwhile, the PLGA tends to be insoluble. Very recently, Lecommandoux and co-workers[26−29] and Schlaad and co-workers[30,31] explored self-assembly behavior of PLGA- and poly(L-lysine) (PLL)-based amphiphilic diblock copolymers in aqueous solution. It was found that vesicles or spherical micelles are formed with different block ratios, and a change in the polypeptide conformation has marked impact on the aggregate size but has no effect on the formed morphologies. The vesicles or spherical micelles do not change when the polypeptide conformation changes. In succession, Savin's group studied the self-assembly behavior of polybutadiene-*b*-poly(L-lysine) in aqueous media and demonstrated a pH-induced morphological transition of rod-to-sphere at low pH values.[32] However, as far as we know, there are few reports on double-responsive polypeptide-based block copolymer self-assembly systems.[36] Temperature and pH are two of the most important external stimuli to the self-assembly system. It is interesting to explore a new type of hydrophilic polypeptide-based copolymer with both temperature and pH sensitivities.

In comparison with the experimental studies, theoretical simulation work regarding the self-assembly behaviors of the block copolymers in solution is limited.[44,45] The great advantage of these studies is that one can obtain a microscopic understanding of the thermodynamic properties and a detailed picture of the self-assembled aggregates. Self-consistent field theory (SCFT) is a powerful technique to understand the complex mesophases experimentally observed for diblock copolymers in both bulk state and dilute solution.[46−54] Recently, our group

* Corresponding author. Tel.: +86-21-64253370. Fax: +86-21-64253539. E-mail: jplinlab@online.sh.cn.

10.1021/jp805072t CCC: $40.75
Published on Web 09/17/2008

has successfully applied the SCFT simulation to the studies of the self-assembly behavior of amphiphilic graft copolymers in dilute solution.[54] The SCFT calculation performed in two dimensions indicated that the molecular structure of the graft copolymer plays an important role in determining the self-assembly behaviors. It is interesting to extend this method to the studies of the self-assembly behavior of ABA type triblock copolymer, which is a model of the PLGA-*b*-PPO-*b*-PLGA.

We report here a study of the self-assembly behaviors of poly(L-glutamic acid)-*b*-poly(propylene oxide)-*b*-poly(L-glutamic acid) (PLGA-*b*-PPO-*b*-PLGA, abbreviated as GPG) with different PLGA block lengths in dilute aqueous solution by both experimental and theoretical methods. We exploited the pH sensitivity of PLGA and thermosensitivity of PPO[55−62] to manipulate the self-assembly structures. The pH determines the secondary structure of PLGA blocks, and the temperature induces the hydration of PPO blocks. The self-assembly behaviors were investigated by transmission electron microscopy (TEM), scanning electron microscopy (SEM), dynamic light scattering (DLS), and circular dichroism (CD). It was found that vesicles transform to spheres when PLGA block length increases or its conformation changes from helix to coil. And increasing the temperature gives rise to a decrease in the size of aggregates. In addition to the experimental studies, we performed SCFT simulations to further verify the micelle structures. The calculations were carried out in three dimensions, which could provide more information about the self-assembled structures than those in two dimensions. By combining experimental and SCFT results, the mechanism regarding the temperature and pH influences on the self-association behaviors of the PLGA-*b*-PPO-*b*-PLGA is proposed.

Experimental Section

Materials. α,ω-Amino poly(propylene oxide) (NH_2−PPO−NH_2, M_w = 4000, Sigma-Aldrich Inc.) was first dissolved with toluene in a flame-dried reaction bottle, followed by removing the toluene in high vacuum to obtain the sample used for copolymer synthesis. Tetrahydrofuran (THF), hexane, 1,4-dioxane were all analytical grade, refluxed with sodium and distilled immediately before use. All other solvents were of analytical grade and used without further purification. The dialysis bag (Membra-cel, 3500 molecular weight cutoff) was provided by Serva Electrophoresis GmbH.

Polymer Synthesis and Characterization. Poly(γ-benzyl-L-glutamate)-*b*-poly(propylene oxide)-*b*-poly(γ-benzyl-L-glutamate) (PBLG-*b*-PPO-*b*-PBLG) triblock copolymers were synthesized by ring-opening polymerization of γ-benzyl-L-glutamate-*N*-carboxyanhydride (BLG-NCA) initiated by NH_2−PPO−NH_2.[63,64] NH_2−PPO−NH_2 and BLG-NCA were dissolved in dioxane separately in two flame-dried reaction bottles, then BLG-NCA solution was added to the solution of NH_2−PPO−NH_2 via a transfer cannula. The reaction was performed at 15 °C under a dry nitrogen atmosphere. After 72 h of stirring, the reaction mixture became a viscous liquid and was poured into a large volume of anhydrous ethanol. The precipitated product was collected and dried under vacuum. The products were purified twice by repeated cycles of dissolution (in chloroform) and precipitation (in anhydrous methanol) of the products. PLGA-*b*-PPO-*b*-PLGA triblock copolymers were prepared by hydrolyzation of PBLG-*b*-PPO-*b*-PBLG with potassium hydroxide (KOH).[42] As a brief, 1 g of PBLG-*b*-PPO-*b*-PBLG was dissolved in 40 mL of THF. In a separate step, an aqueous solution of KOH (3 mol equiv with respect to the benzyl group) was prepared and added to the solution of the polymers. After 4 h of stirring, the mixture was acidulated with excess HCl and dialyzed in distilled water for about 72 h to remove organic solvents and other small impurity. The products were finally freeze-dried to get PLGA-*b*-PPO-*b*-PLGA powder.

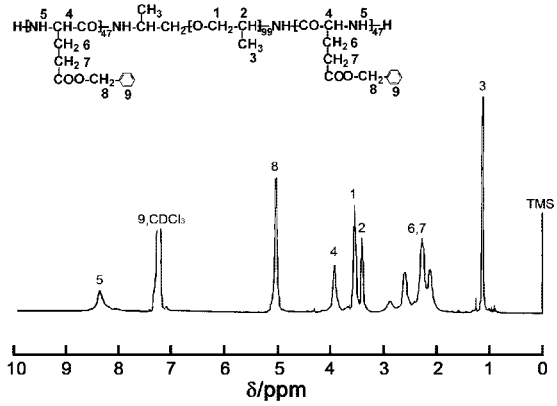

Figure 1. ^{1}H NMR spectrum of PBLG-*b*-PPO-*b*-PBLG triblock copolymer in $CDCl_3$.

TABLE 1: Characteristics of PLGA-*b*-PPO-*b*-PLGA Triblock Copolymers

sample	copolymer[a]	M_n (kg/mol)[b]	PDI[c]
GPG18	$PLGA_{18}$-*b*-PPO_{69}-*b*-$PLGA_{18}$	8.6	1.12
GPG47	$PLGA_{47}$-*b*-PPO_{69}-*b*-$PLGA_{47}$	16.1	1.27
GPG99	$PLGA_{99}$-*b*-PPO_{69}-*b*-$PLGA_{99}$	29.5	1.20

[a] The composition of the copolymers is derived from ^{1}H NMR spectra of the precursor PBLG-*b*-PPO-*b*-PBLG in $CDCl_3$. [b] Number-average molecular weights M_n of PLGA-*b*-PPO-*b*-PLGA are calculated from the composition given in the second column. [c] Polydispersity indexes (PDI = M_w/M_n, where M_w is weight-average molecular weight and M_n is number-average molecular weight) of the precursor PBLG-*b*-PPO-*b*-PBLG are determined by GPC.

The composition of the triblock copolymers before hydrolysis was determined by ^{1}H NMR spectra (Avance 550, Bruker) with $CDCl_3$ as solvent and TMS as the internal reference. A typical ^{1}H NMR spectrum is given in Figure 1. Since the degree of polymerization (DP) of the PPO block is known (69), the total molecular weights of the triblock copolymers can be calculated by the peak intensities of the methylene proton signal (5.1 ppm) of polypeptide and the methylene proton signal (3.6 ppm) of PPO in the ^{1}H NMR spectra. The ^{1}H NMR spectra of obtained GPG triblock copolymers in $CDCl_3$ show that benzyl groups were completely removed after hydrolyzation. This is indicated by the disappearance of methylene proton peak (5.1 ppm) of PBLG segments. The polydispersities of the triblock copolymers before hydrolyzation were determined by gel permeation chromatography (GPC) in dimethylformamide (DMF) at room temperature, performed on a Waters 1515 instrument. Detailed information regarding the characteristics of the GPG triblock copolymers is shown in Table 1.

Sample Preparations. All the GPG triblock copolymers were directly dissolved in 0.1 M KOH aqueous solution to yield 4 mg/mL original solutions. All the solutions showed a blue tint appearance that indicates the formation of the aggregates. The original solutions were diluted to 0.02 mg/mL for TEM, SEM, and DLS testings and 0.2 mg/mL for CD measurements. The pH value of the solutions was carefully adjusted by HCl solution. Before analysis, the solutions were stabilized for more than 5 days.

Transmission Electron Microscopy. The morphologies of the aggregates were examined by TEM (JEM-2000EXII, JEOL)

operated at an accelerating voltage of 60 kV. Drops of solution were placed on a copper grid coated with carbon film and then dried at room temperature. Before the observations, the samples were stained by phosphotungstic acid aqueous solution (0.5 wt %).

Scanning Electron Microscopy. The morphologies of the aggregates were also observed by SEM (JSM 6460, JEOL) operated at an accelerating voltage of 20 kV. The samples were prepared by placing drops of solution on a copper grid coated with carbon film and then drying them at room temperature. Before the observations, the samples were sputtered by carbon.

Dynamic Light Scattering. DLS experiments were performed by using an ALV laser goniometer, with a 22 mW linearly polarized He−Ne laser ($\lambda = 632.8$ nm) and an ALV-5022 multiple tau digital correlator. The measurements were carried out at 20 and 40 °C or otherwise noted. The Laplace inversion of a measured intensity−intensity time correlation function $G^{(2)}(t, q)$ in the self-beating mode can result in a line width distribution G(Γ). For a pure diffusive relaxation, Γ is related to the translational diffusion coefficient D by $(\Gamma/q^2)_{\theta\to 0} \to D$ or a hydrodynamic radius distribution $f(R_h)$

$$R_h = k_B T/(6\pi\eta D) \quad (1)$$

where k_B, T, and η are the Boltzmann constant, the absolute temperature, and the solvent viscosity, respectively. In this study, at a given concentration, $\Gamma/q^2{}_{\theta\to 0}$ or D of the micelles was calculated from the slope by extrapolating q^2 to 0, where q is the magnitude of the scattering wave vector [$q = (4\pi n/\lambda)\sin(\theta/2)$]; n is the solvent refractive index. Then the hydrodynamic radius R_h of the micelles at a given polymer concentration can be further calculated from eq 1.

Circular Dichroism. CD analyses of the secondary structure of the PLGA blocks were performed with a JASCO J810 spectrometer at room temperature. The diluted solutions (0.2 mg/mL) were introduced in quartz cells with 1 cm optical path length. Wavelengths between 200 and 300 nm were analyzed, with an integration time of 1 s and a wavelength step of 0.2 nm.

Self-Consistent Field Theory for ABA Triblock Copolymers in Solution. Below, we provide a brief description of the SCFT framework that we used to probe the self-assembly behavior of ABA amphiphilic triblock copolymers in dilute solution. To mimic the GPG copolymers in solution, we consider a system with volume V, containing n_P ABA triblock copolymers and n_S solvent molecules (S). The triblock copolymers are symmetric, and the total length of copolymer chain is N. The A and B chain length are N_A and N_B, respectively. The A and B segments and solvent are assumed to be incompressible and have a common volume $\rho_0{}^{-1}$. The A and B segments are also assumed to have the statistical lengths a_A and a_B, respectively. f_A denotes the volume fraction of A segment per copolymer chain, and that of B segment is $f_B = 1 - f_A$. The volume fractions of triblock copolymers and solvent molecules in solution are c_P and c_S, respectively.

Within mean-field theory, the pair interactions between the different components are determined by a set of effect chemical potential fields ω_K (K = A, B, S), replacing actual interactions within solution. The free energy of the amphiphilic triblock copolymer system in solution can be given by[46,47]

$$\frac{NF}{\rho_0 k_B T} = -c_P \ln\frac{Q_P}{V} - c_S N \ln\frac{Q_S}{V} - \frac{1}{V}\int d\mathbf{r}[\omega_A(\mathbf{r})\varphi_A(\mathbf{r}) + \omega_B(\mathbf{r})\varphi_B(\mathbf{r}) + \omega_S(\mathbf{r})\varphi_S(\mathbf{r}) - \chi_{AB}N\varphi_A(\mathbf{r})\varphi_B(\mathbf{r}) - \chi_{AS}N\varphi_A(\mathbf{r})\varphi_S(\mathbf{r}) - \chi_{BS}N\varphi_B(\mathbf{r})\varphi_S(\mathbf{r}) + \xi(\mathbf{r})(1 - \varphi_A(\mathbf{r}) - \varphi_B(\mathbf{r}) - \varphi_S(\mathbf{r}))] \quad (2)$$

where k_B is Boltzmann's constant and T is the temperature. Here, $\phi_A(\mathbf{r})$, $\phi_B(\mathbf{r})$, and $\phi_S(\mathbf{r})$, which correspond to the density fields, are the local volume fractions of A segment, B segment, and solvent, respectively. The pressure field $\zeta(\mathbf{r})$ is invoked by incompressibility condition ($\phi_A(\mathbf{r}) + \phi_B(\mathbf{r}) + \phi_S(\mathbf{r}) = 1$). χ_{IJ} characterize the interactions between species I and J. Q_S is the partition function of a solvent molecule in the field $\omega_S(\mathbf{r})$ given by $Q_S = \int d\mathbf{r}\exp(-\omega_S(\mathbf{r})/N)$. $Q_P = \int d\mathbf{r}\, q(\mathbf{r},s)q^+(\mathbf{r},1-s)$ is the partition function for a single noninteracting triblock copolymer chain subject to fields $\omega_A(\mathbf{r})$ and $\omega_B(\mathbf{r})$. The contour length s increases continuously from 0 to 1 as the segment changes from one end to the other. The spatial coordinate $\mathbf{r}$ is in units of $R_{gA} = a_A(N/6)^{1/2}$. The propagator $q(\mathbf{r}, s)$ represents the probability of finding segments s at position $\mathbf{r}$, which satisfies the modified diffusion equation:

$$\frac{\partial q(\mathbf{r},s)}{\partial s} = \frac{a_{\theta(s)}{}^2}{a_A{}^2}\nabla^2 q(\mathbf{r},s) - \omega_{\theta(s)}(\mathbf{r})q(\mathbf{r},s)$$

with the initial condition $q(\mathbf{r}, 0) = 1$. Here, $\theta(s)$ is used to specify the segment type along the copolymer chain, defined by

$$\theta(s) = \begin{cases} A & \text{if} \quad 0 < s < f_A/2 \\ B & \text{if} \quad f_A/2 < s < 1 - f_A/2 \\ A & \text{if} \quad 1 - f_A/2 < s < 1 \end{cases} \quad (3)$$

The backward propagator $q^+(\mathbf{r}, s)$ satisfies the same diffusion equation as $q(\mathbf{r}, s)$ subject to initial condition $q^+(\mathbf{r}, 0) = 1$ due to the symmetric feature of the copolymer chain. The minimization of free energy F, with respect to $\phi_A(\mathbf{r})$, $\phi_B(\mathbf{r})$, $\phi_S(\mathbf{r})$, and $\zeta(\mathbf{r})$, can lead to a set of mean-field equations describing the thermodynamic behavior of copolymers:[54]

$$\omega_A(\mathbf{r}) = \chi_{AB}N\varphi_B(\mathbf{r}) + \chi_{AS}N\varphi_S(\mathbf{r}) + \xi(\mathbf{r}) \quad (4)$$

$$\omega_B(\mathbf{r}) = \chi_{AB}N\varphi_A(\mathbf{r}) + \chi_{BS}N\varphi_S(\mathbf{r}) + \xi(\mathbf{r}) \quad (5)$$

$$\omega_S(\mathbf{r}) = \chi_{AS}N\varphi_A(\mathbf{r}) + \chi_{BS}N\varphi_B(\mathbf{r}) + \xi(\mathbf{r}) \quad (6)$$

$$\varphi_A(\mathbf{r}) + \varphi_B(\mathbf{r}) + \varphi_S(\mathbf{r}) = 1 \quad (7)$$

The details about the numerical calculation of SCFT can be found in our previous studies.[54] The SCFT calculations were implemented in three dimensions on a 64 × 64 × 64 lattice with periodic boundary conditions. Contour step size was set to be 0.01. The numerical simulation was carried out until the relative free energy changes at each iteration were smaller than 10^{-5} and the incompressibility condition was achieved. The initial density fluctuation amplitude was kept at the same value to ensure that the resulting aggregate morphologies were not affect by the initial density fluctuation. In addition, the simulations starting from a homogeneous copolymer solution were repeated for 10−20 times using different initial random states and different random numbers to ensure that the observed phenomena were not accidental.

Results and Discussion

Morphologies Observed by TEM and SEM. Since the PPO blocks are hydrophobic in aqueous solution at room temperature,

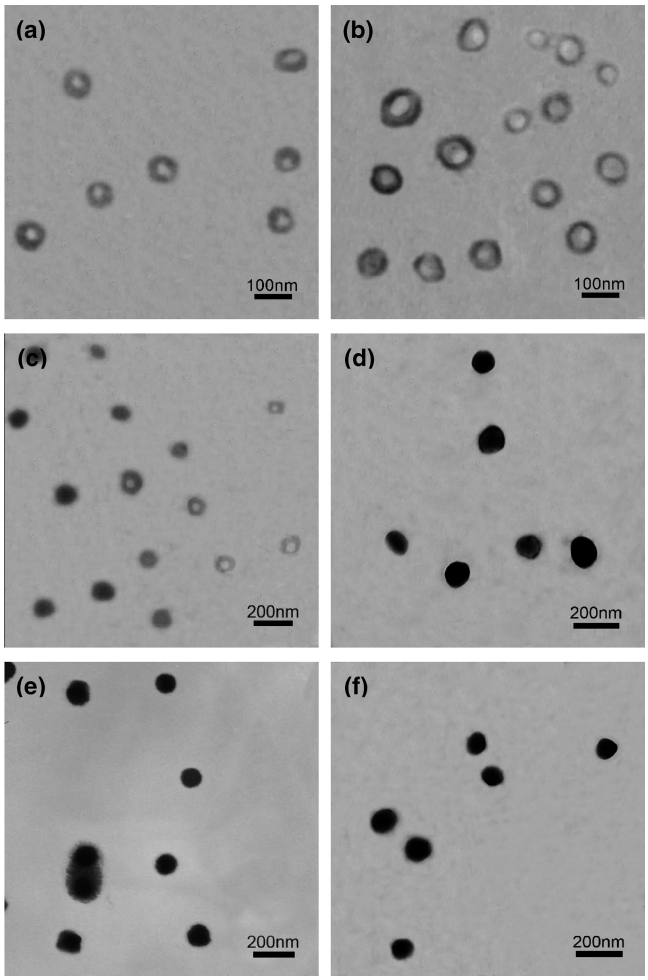

Figure 2. TEM photographs of the GPG aggregates formed in aqueous solution under various conditions: (a) GPG18 at pH = 4.1, (b) GPG18 at pH = 11.5, (c) GPG47 at pH = 4.1, (d) GPG47 at pH = 11.0, (e) GPG99 at pH = 4.0, and (f) GPG99 at pH = 12.0.

self-assembly occurs when the PLGA-*b*-PPO-*b*-PLGA samples were dissolved in water. Figure 2 shows typical TEM photographs of aggregate morphologies formed by GPG triblock copolymers in aqueous solutions. The TEM results show that GPG18 (the "18" denotes the number of L-glutamic acid (LGA) units) forms vesicles at pH = 3.8−12.0. Parts a and b of Figure 2 give the images of GPG18 aggregates at pH values of 4.1 and 11.5, respectively. GPG47 self-assembles into a mixture of spherical micelles and vesicles under acidic conditions (Figure 2c, pH = 4.1). As the pH value increases, the vesicles transform to spheres, and a pure spherical morphology is exhibited under basic conditions (Figure 2d, pH = 11.0). GPG99 produces spheres exclusively in despite the change of the pH value. The typical photographs of GPG99 aggregates at pH = 4.0 and 12.0 are shown in Figure 2, parts e and f. From the above results, we learned that the PLGA block length and pH value are important factors manipulating the aggregate morphology. Vesicles are preferred for the samples with shorter PLGA block length or at lower pH values, whereas they transform to spheres with increasing PLGA length or pH value.

The morphologies of the aggregates were also examined by SEM. Typical images of the vesicles observed for GPG18 at pH = 11.5 and spherical micelles observed for GPG99 at pH = 12.0 are provided in Figure 3. In dry state the vesicles are collapsed and show low inner than the edge (Figure 3a). The spherical micelles have solid structure and give spherical images

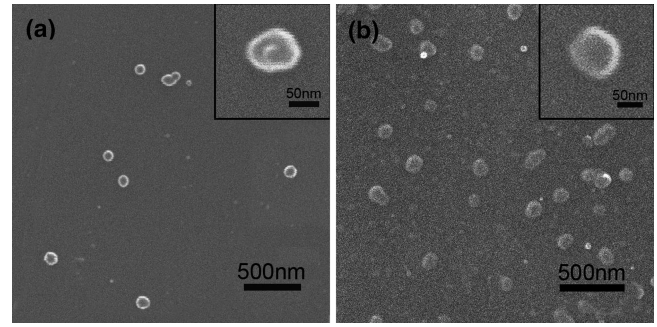

Figure 3. SEM photographs of the GPG aggregates formed in aqueous solution under various conditions: (a) GPG18 at pH = 11.5; (b) GPG99 at pH = 12.0. The insets are high-magnification images.

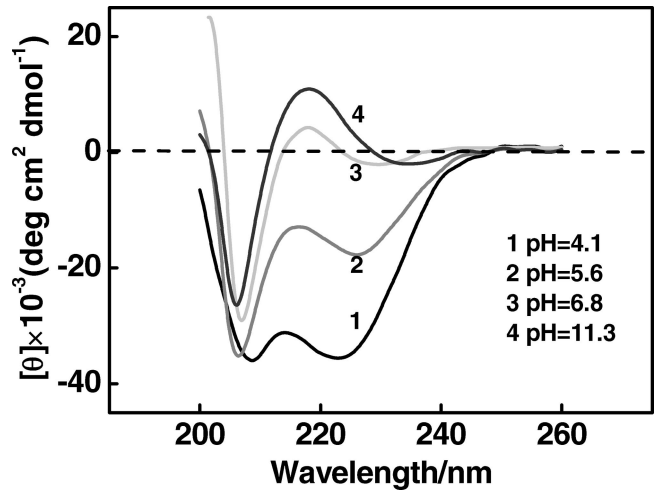

Figure 4. CD spectra for the GPG99 micelle solutions with various pH values.

in SEM observations (Figure 3b). The SEM results are in good agreement with TEM observations.

Conformation of PLGA Chains Characterized by CD. The pH-induced conformational change of polypeptide blocks was investigated by CD. Figure 4 presents the typical CD spectra recorded for GPG99 micelle solutions with various pH values at room temperature. The CD spectrum at pH = 11.3 shows a typical curve with a small positive maximum at 218 nm, characteristic of a random coil conformation. When the pH value is decreased, the intensity of this positive maximum peak starts to decrease obviously at pH = 6.8. Therefore, we concluded that the coil-to-helix transition of PLGA block occurs around pH = 7. This result is in good agreement with the data reported in the literature.[27] When the pH value is decreased to 4.1, two negative minima at 222 and 208 nm could be detected, proving the formation of an α-helix conformation.[65,66] At higher pH values, the polypeptide blocks with coil form are extended due to the electrical repulsion between the PLGA residues. The repulsion decreases as pH value is decreased. At lower pH, the polypeptide blocks with helix form tend to shrink and have lower hydrophilicity.[27,33]

pH and Temperature Dependence of Aggregate Size Studied by DLS. The variation of aggregate structure as functions of pH and temperature were further examined using DLS. As shown in Figure 5, the hydrodynamic radius ($\langle R_h \rangle$) of GPG18 (performed at 25 °C) increases from 140 nm at pH = 4.1 to a maximum value at about pH = 6.7, than decreases to around 130 nm under basic conditions. With increasing pH value, the $\langle R_h \rangle$ of GPG47 decreases first, then the effect of the pH change becomes weak. Concomitantly

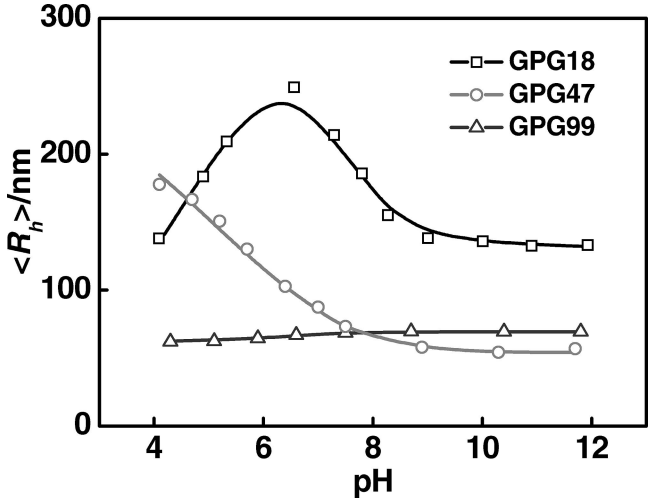

Figure 5. Plots of $\langle R_h \rangle$ of GPG aggregates as a function of pH value.

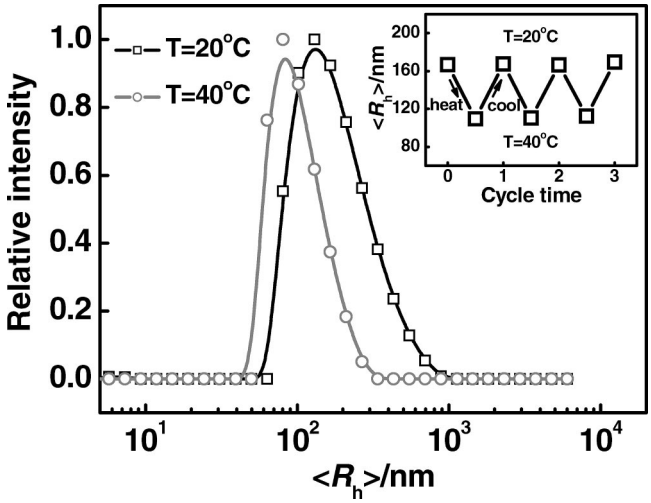

Figure 6. $\langle R_h \rangle$ distribution of GPG47, pH = 4.7 at 20 and 40 °C. Shown in the inset is a plot of the $\langle R_h \rangle$ as a function of thermal treatment process.

with the change in aggregate size, the morphology of the GPG47 aggregates changes from vesicle to spherical micelle. As for the aggregates formed by GPG99, the pH value influences slightly on its aggregate size, it keeps around 60 nm at all the pH values examined. The DLS results of the size of the spherical micelles are in agreement with TEM observations, but the vesicles are much smaller on TEM images than DLS results. This is because that the vesicles could shrink dramatically in dry state. It is worthy to mention that under the present condition employed, the aggregates become colloidal unstable due to the insolubility of the PLGA blocks, when the pH value is less than 3.8.

Figure 6 shows the $\langle R_h \rangle$ distribution of GPG47 aggregate as a function of the temperature at pH = 4.7. The $\langle R_h \rangle$ of GPG47 aggregate at pH = 4.7 is 167 nm at 20 °C. With increasing temperature to 40 °C, the $\langle R_h \rangle$ decreases to 110 nm. The $\langle R_h \rangle$ of the aggregates has a narrower distribution at higher temperature. As shown in the inset, the $\langle R_h \rangle$ value keeps the same within the certain temperature range in several heating−cooling processes. This temperature-dependent effect of $\langle R_h \rangle$ is also shown for the GPG18 and GPG99 samples. The aggregate size decreases with increasing temperature. In addition, the results reveal that the vesicles shrink much more markedly than spherical micelles with increasing temperature. Note that all of the tests on $\langle R_h \rangle$ value were performed after the cell was equilibrated for about 1 h, indicating that the system responds to the temperature stimulation very quickly.

It is well-known that the propylene units of PPO are highly hydrated at low temperature.[55−62] When the propylene units are confined to the interior of the aggregates, the aggregates contain a large water fraction in the aggregate core. The proportion of hydrated propylene units decreases with increasing temperature. The water is gradually excluded from the interior of the aggregates, resulting in a decrease of $\langle R_h \rangle$. The hydration or dehydration of propylene units is very rapid, so the $\langle R_h \rangle$ gets equilibrated in a short time when the temperature varies. At lower temperatures, the chain exchange between aggregates and free chains is rapid, which broadens the $\langle R_h \rangle$ distribution of the aggregates. At higher temperatures, the aggregates are more uniform and stable.

Self-Consistent Field Theory Simulations. As revealed by the experiments, the length of the PLGA blocks and the pH value of the solution exert significant influence on the morphologies of the aggregates. In order to capture the essential feature of GPG triblock copolymer, a model of ABA triblock copolymer was constructed in the SCFT simulations. Increasing the length of PLGA blocks in the experiments corresponds to an increase in the fraction f_A of A block in ABA model triblock copolymer at fixed B block length. The PLGA blocks are in extended coil form at high pH value, because the anionic charges of side-chain carboxyl groups on PLGA blocks exhibit interchain repulsions. The electrostatic repulsions disappear due to the protonation of PLGA blocks under acidic condition, which results in a shrinkage of the PLGA blocks at lower pH values. Thus, the change of pH value from basic to acidic conditions causes a decrease in the statistical length a_A of PLGA blocks. Since the pH value has weak impact on the PPO blocks, the ratio a_A/a_B could become small as the pH value decreases. Meanwhile, the variation in pH value also changes the local interactions between various species, which are described by the classical Flory−Huggins parameters (χ). Since PLGA block is soluble in basic condition, a negative χ_{AS} value of −0.175 was adopted to simulate the experimental morphology. When the pH value is decreased, PLGA tends to be insoluble. Therefore, a positive χ_{AS} value of 0.075 was used, corresponding to the change in the solubility. Because the interaction between PLGA block (A block) and solvent (S) plays a major role in determining the morphological change, and also for the simplicity of the calculations, we do not consider the variation of the interaction parameters between PPO (B block) and solvent χ_{BS}, and PLGA (A block) and PPO (B block) χ_{AB}, when the pH value changes. χ_{BS} was set to be 1.70 in accord with the insoluble nature of PPO block (B block), whereas χ_{AB} was set to be 0.50 due to the incompatibility between A and B blocks. In present simulations, the volume fraction c_P of triblock copolymers in solution was set to be 0.08. The length N_B of the B chain of triblock copolymer was assumed to be 32; thus, that of total length of triblock copolymer chain is $32/(1-f_A)$.

Figure 7 shows aggregate morphological changes of ABA triblock copolymers in dilute solution with increasing the volume fraction of hydrophilic blocks. The red and blue colors are assigned to indicate the B and A blocks, respectively. The solvent is not illustrated for clarification. As can be seen, with increasing f_A, the aggregate morphologies transform from vesicles to a mixture of spherical micelles and vesicles, then to pure spherical micelles.

Figure 8 shows aggregate morphologies of amphiphilic ABA triblock copolymers in dilute solution with various values of

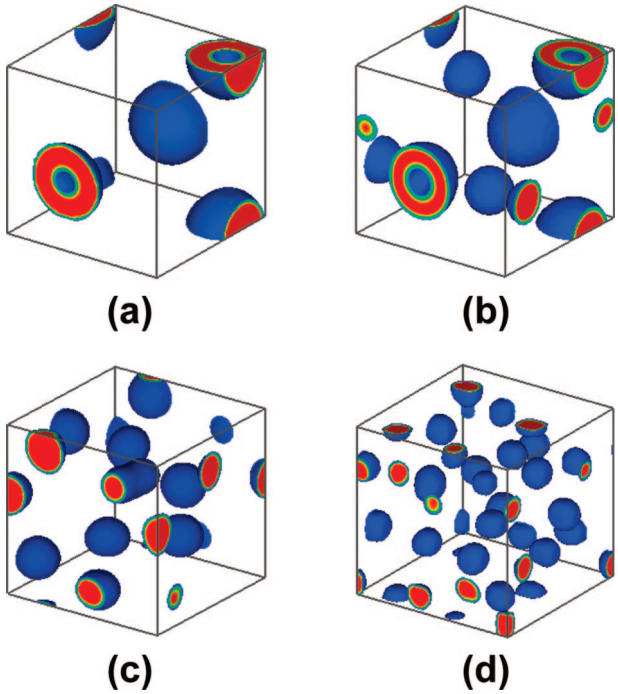

Figure 7. Aggregate morphologies of amphiphilic ABA triblock copolymers in dilute solution with an increase in the volume fraction f_A of A blocks: (a) $f_A = 0.111$, (b) $f_A = 0.158$, (c) $f_A = 0.256$, and (d) $f_A = 0.396$, at $a_A/a_B = 1.0$, $N_B = 32$, $\chi_{AB} = 0.50$, $\chi_{AS} = -0.175$, $\chi_{BS} = 1.70$. The red and blue colors are assigned to indicate the B and A blocks, respectively. The solvent is not illustrated for clarification.

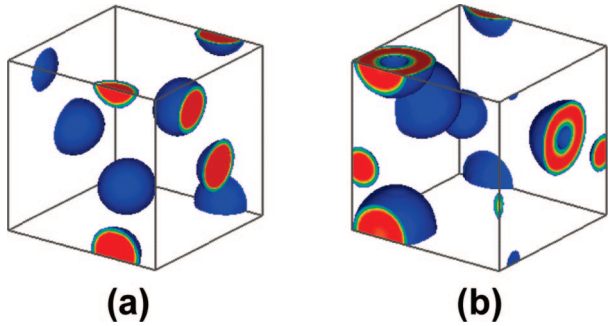

Figure 8. Aggregate morphologies of amphiphilic ABA triblock copolymers in dilute solution at $f_A = 0.200$, $N_B = 32$, $\chi_{AB} = 0.50$, $\chi_{BS} = 1.70$. (a) $\chi_{AS} = -0.175$, $a_A/a_B = 1.0$; (b) $\chi_{AS} = 0.075$, $a_A/a_B = 0.8$. The red and blue colors are assigned to indicate the B and A blocks, respectively. The solvent is not illustrated for clarification.

the ratio of a_A to a_B and interaction parameter χ_{AS}. The pure spherical micelles are observed at $\chi_{AS} = -0.175$ and $a_A/a_B = 1.0$ (Figure 8a). As the parameters change to $\chi_{AS} = 0.075$, $a_A/a_B = 0.8$, the aggregate morphologies transform from pure micelles to a mixture of micelles and vesicles (Figure 8b).

The SCFT results can also provide the microscopic information regarding the self-association, which cannot be obtained by experiments. For example, the important density distributions of hydrophilic blocks ϕ_A and hydrophobic blocks ϕ_B in vesicle and sphere are plotted in Figure 9. The insets illustrate the two-dimensional density profiles of hydrophobic blocks. Figure 9a shows the typical density distribution for a sphere. The hydrophobic blocks aggregate in the core of the sphere, and the hydrophilic blocks are localized at the corona region of sphere. For the vesicles, the profile of ϕ_B shows a bimodal feature (as shown in Figure 9b), i.e., the hydrophobic blocks B form the wall of the vesicle. The inner and outer leaves of the vesicle are composed of the hydrophilic blocks A. The density

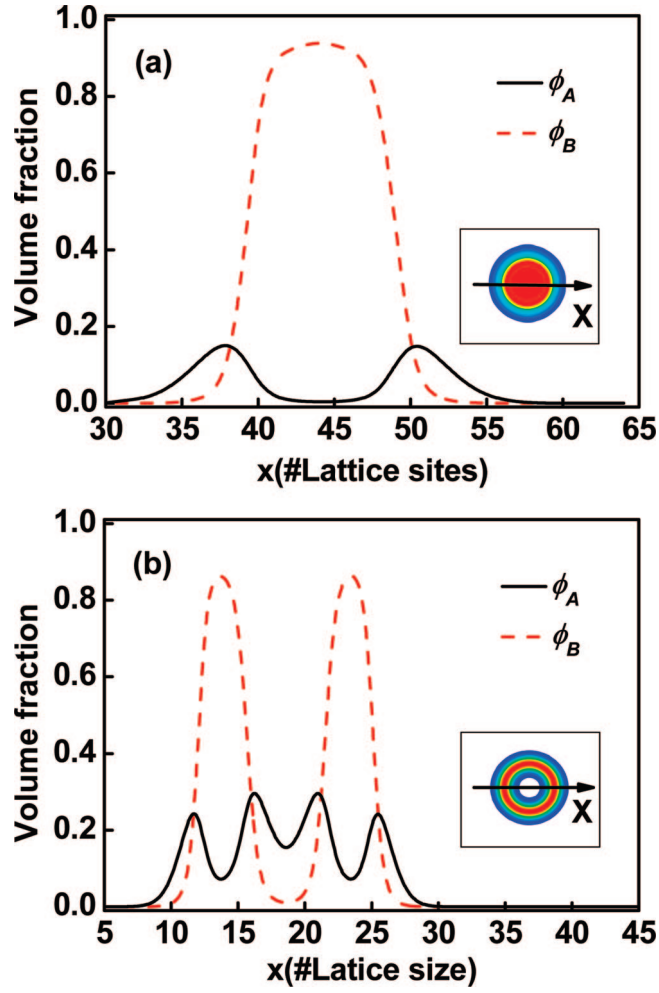

Figure 9. Density distribution profiles of hydrophilic A blocks ϕ_A and hydrophobic B blocks ϕ_B on a cross section of the aggregate marked with an arrow in the inset: (a) spherical micelle, $a_A/a_B = 1.00$ and $f_A = 0.256$; (b) vesicle, $a_A/a_B = 1.00$ and $f_A = 0.158$. The insets are the two-dimensional density distributions of hydrophobic B blocks, where the density of B block increases as the color changes from blue to red.

peaks of hydrophilic blocks in the outer leaf are lower than those in the inner leaf.

The simulation results are qualitatively consistent with the general features of these experimental findings. In our experiments, the structural transition of self-aggregates as a function of the length of PLGA blocks, corresponding to the parameter f_A in the model, was investigated. As the PLGA block length increases progressively, at higher pH values, the GPG18, GPG47, and GPG99 self-assemble into vesicles, a mixture of spherical micelles and vesicles, and spherical micelles, respectively (as shown in Figure 2). As illustrated in Figure 7, the transition sequences of vesicles → a mixture of spherical micelles and vesicles → spherical micelles are demonstrated. It should be noted that the main reason for the coexistence of spherical micelles and vesicles in the present work is the thermodynamic phenomenon, as revealed by the SCFT calculations. The polydispersity could have some effect on the morphological stability region.[48] However, the general feature of the aggregation is not changed.

We also exploited the pH value to tailor the aggregate morphologies in dilute solution. GPG47 self-assembles into pure spherical micelles under basic conditions, which is in good agreement with the SCFT prediction as shown in Figure 8a. As

SCHEME 1: Schematic Representation of the Structure Change of PLGA-*b*-PPO-*b*-PLGA Aggregates from Spherical Micelles (a) to Vesicles with Decreasing the PLGA Block Length (b) or Decreasing pH Value of Solution (c)

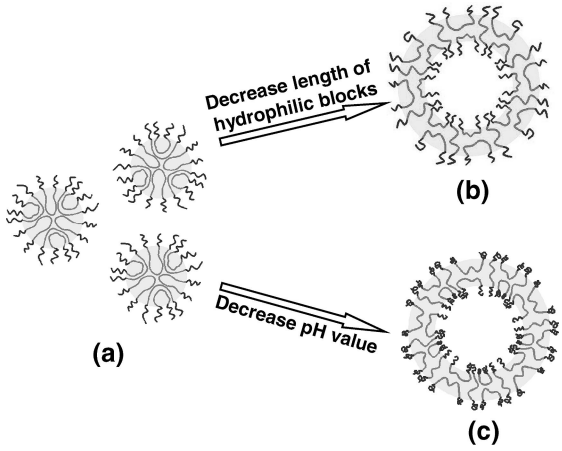

the pH value decreases, a mixture of vesicles and spherical micelles is shown. To mimic the pH effect on self-assembly behavior of amphiphilic copolymers, the statistical length of PLGA blocks and Flory−Huggins parameter between PLGA blocks and solvent are changed accordingly in the simulations, and a morphology of vesicles in coexistence with spheres was reproduced in the simulations (as shown in Figure 8b).

The SCFT, which was originated from the field theoretical approach of Edwards, has emerged as a powerful tool to study the equilibrium thermodynamical features of polymers.[46] Recently, this theory was successfully extended to investigate the aggregation behavior of amphiphilic block copolymers in dilute solution.[47−52] The subject studied in present work demonstrates that the self-association behaviors of PLGA-*b*-PPO-*b*-PLGA were well reproduced by the SCFT calculations after the length and the conformation of PLGA block were lumped into the fraction and the statistical length of the hydrophobic block of model ABA triblock copolymer.

Summarizing both the experimental findings and SCFT results, we propose the mechanism of the structure change of the PLGA-*b*-PPO-*b*-PLGA aggregates. Shown in Scheme 1 is the schematic illustration of the aggregates formed under different conditions. The PLGA-*b*-PPO-*b*-PLGA triblock copolymers self-associate to form spherical micelles when the PLGA hydrophilic blocks are longer or in basic surroundings where PLGA takes a flexible extended chain form (Scheme 1a). These are manifested by the spheres formed by GPG99 and GPG47 in basic surroundings. The hydrophobic PPO chains form the micelle core, whereas the PLGA blocks form the corona. Such structures are firmly verified by the SCFT simulations (Figures 7 and 8). When the chain length of the PLGA becomes shorter or PLGA tends to shrink in the coil-to-helix transition, vesicles are formed. The free energy penalty associated with the shortening or shrinking of the hydrophilic PLGA chains is compensated by the reducing of the interfacial area between hydrophilic and hydrophobic areas within the aggregates upon the spherical micelle to vesicle transition. The vesicles are illustrated in Scheme 1, parts b and c, where the PPO chains form the wall and the PLGA blocks form the leaf according to the SCFT results. In addition to the structural sensitivity to the PLGA chain length and pH value, the formed aggregates are also temperature-responsive. The aggregates become compact at higher temperatures owing to the dehydration of the PPO blocks.

We present a first example, to our best knowledge, of polypeptide-based triblock copolymer which can undergo structural change from vesicle to spheres upon changing pH value. Spherical micelles and vesicles have been found for the polypeptide-based diblock copolymers. Changing the pH value has an impact on the secondary structure of the polypeptide blocks. However, it was not found that the morphology of the aggregates (spherical micelles or vesicles) changes when the pH of solution varies.[67] In addition to pH sensitivity, the aggregates formed by PLGA-*b*-PPO-*b*-PLGA are also sensitive to temperature. Such characteristics may find potential applications in clinical treatments. For example, the temperature and pH value of tissues with pathological changes are usually slightly different from the normal values. Due to the biocompatible nature of the polypeptide, the aggregates with both temperature- and pH-responsive behavior may serve as an ideal drug carrier for the controlled release. Rapid release rates can be achieved in the pathological change areas with abnormal temperature and pH value by regulating the GPG aggregates structures. The GPG self-assembled systems may act as suitable drug carriers with smart controlled release behavior in the applications of drug delivery systems.

Conclusion

The pH- and thermosensitive PLGA-*b*-PPO-*b*-PLGA triblock copolymers were synthesized by ring-opening polymerization of BLG-NCA initiated by $NH_2-PPO-NH_2$. Their self-assembly behaviors in dilute solution were studied by combining experimental methods and SCFT simulations. Experimental results showed that the vesicles transform to spherical micelles when hydrophilic PLGA block length increases. Also, vesicles can transform to spherical micelles when conformation of PLGA blocks changes from helix to coil, which depends on the pH value of solution. The aggregate size decreases as the temperature increases. This is attributed to the dehydration of the PPO blocks at high temperatures. In the theoretical studies, the length and the conformation of PLGA blocks, which are important factors affecting the aggregate morphology, were lumped into the fraction and the statistical length of hydrophilic A blocks of model ABA triblock copolymer, respectively. The aggregate morphology transforms from vesicles to spherical micelles with increasing the fraction or statistical length of hydrophilic A blocks. The simulation results are in good agreement with the experimental findings.

Acknowledgment. This work was supported by the National Natural Science Foundation of China (50673026, 20574018). Support from the Doctoral Foundation of the Education Ministry of China (Grant No. 20050251008) and Projects of the Shanghai Municipality (06SU07002, 0652nm021, 082231, and B502) are also appreciated.

References and Notes

(1) Zhang, L.; Yu, K.; Eisenberg, A. *Science* **1996**, *272*, 1777.
(2) Zhang, L.; Eisenberg, A. *Macromolecules* **1996**, *29*, 8805.
(3) Jenekhe, S. A.; Chen, X. L. *Science* **1998**, *279*, 1903.
(4) Chen, Z.; Cui, H.; Hales, K.; Li, Z.; Qi, K.; Pochan, D. J.; Wooley, K. L. *J. Am. Chem. Soc.* **2005**, *127*, 8592.
(5) Kim, J.-K.; Lee, E.; Huang, Z.; Lee, M. *J. Am. Chem. Soc.* **2006**, *128*, 14022.

(6) Förster, S.; Hermsdorf, N.; Leube, W.; Schnablegger, H.; Regenbrecht, M.; Akari, S.; Lindner, P.; Böttcher, C. *J. Phys. Chem. B* **1999**, *103*, 6657.
(7) Cornelissen, J. J. L. M.; Fischer, M.; Sommerdijk, N. A. J. M.; Nolte, R. J. M. *Science* **1998**, *280*, 1427.
(8) Wang, X.; Guerin, G.; Wang, H.; Wang, Y.; Manners, I.; Winnik, M. A. *Science* **2007**, *317*, 644.
(9) Tang, D.; Lin, J.; Lin, S.; Zhang, S.; Chen, T.; Tian, X. *Macromol. Rapid Commun.* **2004**, *25*, 1241.
(10) Riess, G. *Prog. Polym. Sci.* **2003**, *28*, 1107.
(11) Moffitt, M.; Eisenberg, A. *Macromolecules* **1997**, *30*, 4363.
(12) Rolland, A.; O'Mullane, J.; Goddard, P.; Brookman, L.; Petrak, K. *J. Appl. Polym. Sci.* **1992**, *44*, 1195.
(13) Kitahara, A. *Adv. Colloid Interface Sci.* **1980**, *12*, 109.
(14) Sauer, M.; Meier, W. *Chem. Commun.* **2001**, *1*, 55.
(15) Gohy, J.-F.; Willet, N.; Varshney, S.; Zhang, J.-X.; Jérôme, R. *Angew. Chem., Int. Ed.* **2001**, *40*, 3214.
(16) Rodríguez-Hernández, J.; Chécot, F.; Gnanou, Y.; Lecommandoux, S. *Prog. Polym. Sci.* **2005**, *30*, 691.
(17) Liu, S.; Billingham, N.; Armes, S. *Angew. Chem., Int. Ed.* **2001**, *40*, 2328.
(18) André, X.; Zhang, M.; Müller, A. E. H. *Macromol. Rapid Commun.* **2005**, *26*, 558.
(19) Li, G.; Shi, L.; Ma, R.; An, Y.; Huang, N. *Angew. Chem., Int. Ed.* **2006**, *45*, 4959.
(20) Jiang, X.; Ge, Z.; Xu, J.; Liu, H.; Liu, S. *Biomacromolecules* **2007**, *8*, 3184.
(21) Ge, Z.; Xie, D.; Chen, D.; Jiang, X.; Zhang, Y.; Liu, H.; Liu, S. *Macromolecules* **2007**, *40*, 3538.
(22) Li, G.; Song, S.; Guo, L.; Ma, S. *J. Polym. Sci., Part A: Polym. Chem.* **2008**, *46*, 5028.
(23) Mountrichas, G.; Pispas, S. *J. Polym. Sci., Part A: Polym. Chem.* **2007**, *45*, 5790.
(24) Mountrichas, G.; Pispas, S. *Macromolecules* **2006**, *39*, 4767.
(25) Pispas, S. *J. Polym. Sci., Part A: Polym. Chem.* **2006**, *44*, 606.
(26) Chécot, F.; Rodríguez-Hernández, J.; Gnanou, Y.; Lecommandoux, S. *Polym. Adv. Technol.* **2006**, *17*, 782.
(27) Chécot, F.; Brûlet, A.; Oberdisse, J.; Gnanou, Y.; Mondain-Monval, O.; Lecommandoux, S. *Langmuir* **2005**, *21*, 4308.
(28) Chécot, F.; Lecommandoux, S.; Klok, H.-A.; Gnanou, Y. *Eur. Phys. J. E* **2003**, *10*, 25.
(29) Chécot, F.; Lecommandoux, S.; Gnanou, Y.; Klok, H.-A. *Angew. Chem., Int. Ed.* **2002**, *41*, 1339.
(30) Kukula, H.; Schlaad, H.; Antonietti, M.; Förster, S. *J. Am. Chem. Soc.* **2002**, *124*, 1658.
(31) Sigel, R.; Losik, M.; Schlaad, H. *Langmuir* **2007**, *23*, 7196.
(32) Gebhardt, K. E.; Ahn, S.; Venkatachalam, G.; Savin, D. A. *Langmuir* **2007**, *23*, 2851.
(33) Sun, J.; Deng, C.; Chen, X.; Yu, H.; Tian, H.; Sun, J.; Jing, X. *Biomacromolecules* **2007**, *8*, 1013.
(34) Sun, J.; Chen, X.; Deng, C.; Yu, H.; Xie, Z.; Jing, X. *Langmuir* **2007**, *23*, 8308.
(35) Babin, J.; Rodríguez-Hernández, J.; Lecommandoux, S.; Klok, H.-A.; Achard, M.-F. *Faraday Discuss.* **2005**, *128*, 179.
(36) Rao, J.; Luo, Z.; Ge, Z.; Liu, H.; Liu, S. *Biomacromolecules* **2007**, *8*, 3871.
(37) Li, T.; Lin, J.; Chen, T.; Zhang, S. *Polymer* **2006**, *47*, 4485.
(38) Matsusaki, M.; Waku, T.; Kaneko, T.; Kida, T.; Akashi, M. *Langmuir* **2006**, *22*, 1396.
(39) Tian, H.; Deng, C.; Lin, H.; Sun, J.; Deng, M.; Chen, X.; Jing, X. *Biomaterials* **2005**, *26*, 4209.
(40) Lavasanifar, A.; Samuel, J.; Kwon, G. S. *Adv. Drug Delivery Rev.* **2002**, *54*, 169.
(41) Holowka, E. P.; Pochan, D. J.; Deming, T. J. *J. Am. Chem. Soc.* **2005**, *127*, 12423.
(42) Rodríguez-Hernández, J.; Lecommandoux, S. *J. Am. Chem. Soc.* **2005**, *127*, 2026.
(43) Wong, M. S.; Cha, J. N.; Choi, K.-S.; Deming, T. J.; Stucky, G. D. *Nano Lett.* **2002**, *2*, 583.
(44) Srinivas, G.; Nielsen, S. O.; Moore, P. B.; Klein, M. L. *J. Am. Chem. Soc.* **2006**, *128*, 848.
(45) Lin, S.; Numasawa, N.; Nose, T.; Lin, J. *Macromolecules* **2007**, *40*, 1684.
(46) Drolet, F.; Fredrickson, G. H. *Phys. Rev. Lett.* **1999**, *83*, 4317.
(47) He, X.; Liang, H.; Huang, L.; Pan, C. *J. Phys. Chem. B* **2004**, *108*, 1731.
(48) Zhu, J.; Jiang, Y.; Liang, H.; Jiang, W. *J. Phys. Chem. B* **2005**, *109*, 8619.
(49) Jiang, Y.; Chen, T.; Ye, F.; Liang, H.; Shi, A.-C. *Macromolecules* **2005**, *38*, 6710.
(50) Wang, R.; Tang, P.; Qiu, F.; Yang, Y. *J. Phys. Chem. B* **2005**, *109*, 17120.
(51) Li, X.; Tang, P.; Qiu, F.; Zhang, H.; Yang, Y. *J. Phys. Chem. B* **2006**, *110*, 2024.
(52) Zhang, L.; Lin, J.; Lin, S. *Macromolecules* **2007**, *40*, 5582.
(53) Zhang, L.; Lin, J.; Lin, S. *J. Phys. Chem. B* **2007**, *111*, 351.
(54) Zhang, L.; Lin, J.; Lin, S. *J. Phys. Chem. B* **2007**, *111*, 9209.
(55) Nivaggioli, T.; Tsao, B.; Alexandridis, P.; Hatton, T. A. *Langmuir* **1995**, *11*, 119.
(56) Jain, N. J.; Aswal, V. K.; Goyal, P. S.; Bahadur, P. *J. Phys. Chem. B* **1998**, *102*, 8452.
(57) Su, Y.; Wang, J.; Liu, H. *Langmuir* **2002**, *18*, 5370.
(58) Alexandridis, P.; Nivaggioli, T.; Hatton, T. A. *Langmuir* **1995**, *11*, 1468.
(59) Zhou, Z.; Chu, B. *J. Colloid Interface Sci.* **1988**, *126*, 171.
(60) Su, Y.; Wang, J.; Liu, H. *J. Phys. Chem. B* **2002**, *106*, 11823.
(61) Su, Y.; Wang, J.; Liu, H. *J. Colloid Interface Sci.* **2002**, *251*, 417.
(62) Goldmints, I.; von Gottberg, F. K.; Smith, K. A.; Hatton, T. A. *Langmuir* **1997**, *13*, 3659.
(63) Lin, J.; Abe, A.; Furuya, H.; Okamoto, S. *Macromolecules* **1996**, *29*, 2584.
(64) Lin, J.; Liu, N.; Chen, J.; Zhou, D. *Polymer* **2000**, *41*, 6189.
(65) Myer, Y. P. *Macromolecules* **1969**, *2*, 624.
(66) Johnson, W. C.; Tinoco, I. *J. Am. Chem. Soc.* **1972**, *94*, 4389.
(67) Börner, H. G.; Schlaad, H. *Soft Matter* **2007**, *3*, 394.

JP805072T